GPS Solut
DOI 10.1007/s10291-017-0660-3

ORIGINAL ARTICLE

GLONASS inter-frequency phase bias rate estimation by single-epoch or Kalman filter algorithm

Yibin Yao[1,2,3] · Mingxian Hu[1] · Xiayan Xu[4] · Yadong He[1]

Received: 23 April 2017 / Accepted: 18 August 2017

Abstract GLONASS double-differenced (DD) ambiguity resolution is hindered by the inter-frequency bias (IFB) in GLONASS observation. We propose a new algorithm for IFB rate estimation to solve this problem. Although the wavelength of the widelane observation is several times that of the $L1$ observation, their IFB errors are similar in units of meters. Based on this property, the new algorithm can restrict the IFB effect on widelane observation within 0.5 cycles, which means the GLONASS widelane DD ambiguity can be accurately fixed. With the widelane integer ambiguity and phase observation, the IFB rate can be estimated using single-epoch measurements, called the single-epoch IFB rate estimation algorithm, or using the Kalman filter to process all data, called the Kalman filter-based IFB rate estimation algorithm. Due to insufficient accuracy of the IFB rate estimated from widelane observations, the IFB rate has to be further refined with $L1$ and $L2$ observations. A new reference satellite selection method is proposed to serve the IFB rate estimation. The experiment results show that the IFB rates on $L1$ and $L2$ bands are different, that an accurate IFB rate will help us to obtain more fixed solutions at places with serious occlusion, that the single-epoch IFB rate estimation algorithm can meet the requirements for real-time kinematic positioning with only 8% extra computational time, and that the Kalman filter-based IFB rate estimation algorithm is a satisfactory option for high-accuracy GLONASS positioning.

Keywords Multi-global navigation satellite system (GNSS) · Real-time kinematic (RTK) positioning · GLONASS integer ambiguity resolution · Inter-frequency bias (IFB)

Introduction

GPS real-time kinematic (RTK) has become a reliable and widespread algorithm for accurate positioning. Fixing ambiguities is necessary to obtain coordinates with centimeter-level accuracy. However, for GLONASS, there is a challenge hindering ambiguity fixing. With various hardware designs, the receiver hardware delay cannot be removed in single-differenced observations among receivers. Furthermore, due to the frequency division multiple access (FDMA) strategy, GLONASS signal wavelengths are unequal, and the receiver hardware delay cannot be eliminated in double-differenced (DD) observations. Thus, for two receivers designed by different manufacturers, there is a residual receiver hardware delay, i.e., an inter-frequency bias (IFB) in the GLONASS DD phase and pseudorange observations. If the IFB cannot be removed or eliminated, it becomes impossible to fix DD ambiguity for most GLONASS phase observation.

There have been a number of attempts to eliminate the effect of the IFB. Pratt et al. (1998) and Wanninger and Wallstab-Freitag (2007) argued that the IFB is frequency dependent and linearly correlated with the frequency

✉ Yibin Yao
ybyao@whu.edu.cn

1 School of Geodesy and Geomatics, Wuhan University, Wuhan 430079, China

2 Key Laboratory of Geospace Environment and Geodesy, Ministry of Education, Wuhan University, Wuhan 430079, China

3 Collaborative Innovation Center for Geospatial Technology, Wuhan 430079, China

4 GNSS Research Center, Wuhan University, Wuhan 430079, China

Published online: 30 August 2017

number (FN) of GLONASS satellites; therefore, one can use an IFB rate with respect to the frequency number instead of the IFB. Wanninger (2012) proved that the IFB rate on $L1$ and $L2$ bands is equal, and the IFB rate is $<$10 cm/FN mostly, but the IFB rate estimation method needs an a priori IFB rate as a precondition. Al-Shaery et al. (2013) estimated the IFB rates of carrier phase and pseudorange observation, and their GPS + GLONASS RTK experiment showed the ambiguity fixed rate increases significantly by using the estimated IFB rate. However, the IFB rate used in the experiment was estimated from a zero baseline in advance, which is difficult to employ widely. Tian et al. (2015) presented a method for the real-time estimated IFB rate based on a particle filter, which can be used in RTK positioning. However, the performance of this algorithm is unreliable when there are few GLONASS satellites tracked, and because the method is exhaustive, the computational efficiency is unsatisfactory.

Therefore, to efficiently, reliably and accurately estimate the IFB rate in real time, a new algorithm is presented in this study. The new algorithm estimates the IFB rate based on widelane and uncombined $L1$ and $L2$ ($L1 + L2$) phase and pseudorange observations. Whereas the widelane wavelength is several multiples of the $L1$ observation, its IFB error is similar to that of the $L1$ observation in units of meters. Based on this property of widelane observation, the new algorithm can restrict the IFB effect on widelane observation within 0.5 cycles; it means the GLONASS widelane DD ambiguity can be fixed accurately. Using the widelane integer DD ambiguity and phase observation, the IFB rate can be estimated by the new algorithm. Due to the different estimation strategy, this method can provide a single-epoch estimated IFB rate and filter estimated IFB rate for different demands. In summary, four experiments proved that the performance of this algorithm is satisfactory. In this contribution, the inter-frequency pseudorange bias is ignored.

Mathematical modeling

For GPS RTK positioning, ionospheric delay, tropospheric delay, satellite clock bias, satellite orbit bias, receiver clock bias, and receiver hardware delay can be reduced or eliminated in the DD phase and code observation. The GPS double-differenced observation equation in units of meters is as follows,

$$\begin{aligned} P_{rm}^{\mathrm{GPS},ij} &= \rho_{rm}^{ij} + \varepsilon(P_{rm}^{\mathrm{GPS},ij}) \\ \Phi_{rm}^{\mathrm{GPS},ij} &= \rho_{rm}^{ij} + \lambda N_{rm}^{ij} + \varepsilon(\Phi_{rm}^{\mathrm{GPS},ij}) \end{aligned} \tag{1}$$

where $P_{rm}^{\mathrm{GPS},ij}$, $\Phi_{rm}^{\mathrm{GPS},ij}$, ρ_{rm}^{ij} and N_{rm}^{ij} refer to the DD pseudorange, DD phase, geometric DD distance and DD ambiguity between satellites i and j and receivers r and m, respectively. λ is the signal wavelength of the GPS satellite, and $\varepsilon(P_{rm}^{\mathrm{GPS},ij})$ and $\varepsilon(\Phi_{rm}^{\mathrm{GPS},ij})$ represent the observation noise and multipath error in the pseudorange and carrier phase observations.

Due to FDMA technology, the signal wavelength of GLONASS satellites differs, and the GLONASS DD ambiguity in units of meters loses its integer property. To recover the integer property, GLONASS DD ambiguity will be transformed as follows (Takasu and Yasuda 2009):

$$\begin{aligned} \lambda^i N_m^i - \lambda^j N_m^j - \lambda^i N_r^i - \lambda^j N_r^j &= \lambda^i N_{rm}^i - \lambda^j N_{rm}^j \\ &= \lambda^i N_{rm}^i - \lambda^i N_{rm}^j + \lambda^i N_{rm}^j - \lambda^j N_{rm}^j \\ &= \lambda^i N_{rm}^{ij} + (\lambda^i - \lambda^j) N_{rm}^j \end{aligned} \tag{2}$$

where i and j are satellites and r and m refer to receivers, in which satellite j is the reference satellite, and receiver r is the base station receiver. N_m^i, N_{rm}^i and N_{rm}^{ij} are the undifferenced ambiguity, single-differenced ambiguity and double-differenced ambiguity. λ^i presents the signal wavelength of GLONASS satellite i.

The receiver hardware delay is composed of a constant offset and an offset related to the frequency (Pratt et al. 1998; Wanninger and Wallstab-Freitag 2007). For receivers from different manufacturers, the GLONASS DD observation still contains double-differenced receiver hardware delay, which can be presented by the IFB rate with respect to the frequency number, as follows:

$$\begin{aligned} &\big((a + k^i\zeta_r) - (a + k^j\zeta_r)\big) - \big((b + k^i\zeta_m) - (b + k^j\zeta_m)\big) \\ &\quad = (k^i - k^j)(\zeta_r - \zeta_m) = (k^i - k^j)\zeta_{rm} \end{aligned} \tag{3}$$

where a and b refer to the constant offset of receivers r and m. ζ_r and ζ_m are the offset that depend on the frequency of receivers r and m. k^j presents the frequency number of receiver j. The IFB rate ζ_{rm} is the difference between the offsets ζ_r and ζ_m.

Thus, the GLONASS double-differenced observation equations in units of meters are as follows:

$$\begin{aligned} P_{rm}^{\mathrm{GLO},ij} &= \rho_{rm}^{ij} + \varepsilon(P_{rm}^{\mathrm{GLO},ij}) \\ \Phi_{rm}^{\mathrm{GLO},ij} &= \rho_{rm}^{ij} + \lambda^i N_{rm}^{ij} + (\lambda^i - \lambda^j) N_{rm}^j + (k^i - k^j)\zeta_{rm} + \varepsilon(\Phi_{rm}^{\mathrm{GLO},ij}) \end{aligned} \tag{4}$$

From observation (4), the IFB rate ζ_{rm}, station coordinates and DD ambiguity N_{rm}^{ij} need to be estimated. The single-differenced ambiguity N_{rm}^j could be calculated by pseudorange and phase observation (Wang 2000).

Since there are no common frequencies between GPS and GLONASS signals, separate reference satellites are selected to form the DD observation for the GPS and GLONASS systems.

New algorithm for GLONASS IFB rate estimation

In this section, the advantage of widelane phase observation on GLONASS IFB rate estimation will be derived and proved. Based on this advantage, two new algorithms for GLONASS IFB rate estimation are presented. The single-epoch IFB rate estimation algorithm can provide IFB rate in real time for RTK, with only one epoch of GNSS observation. The Kalman filter-based IFB rate estimation can estimate a very accurate GLONASS IFB rate using GNSS observations of all epochs.

Theory of the new algorithm

The widelane phase observation is a linear combination of $L1$ and $L2$ phase observations in units of meters as follows:

$$\phi^{ij}_{rm_{\mathrm{WL}}} = \left(\phi^{ij}_{rm_{L1}}/\lambda_{L1} - \phi^{ij}_{rm_{L2}}/\lambda_{L2}\right)\lambda_{\mathrm{WL}} \tag{5}$$

where $\phi^{ij}_{rm_{\mathrm{WL}}}$ refers to the widelane DD phase observation between satellites i and j and receivers r and m, and λ_{L1} is the wavelength of $L1$ phase observation.

Because the widelane phase observation is a linear combination of the $L1$ and $L2$ phase observation, the IFB of the widelane observation can be computed as follows:

$$\begin{aligned}\zeta_{rm_{\mathrm{WL}}} &= \left(\zeta_{rm_{L1}}/\lambda_{L1} - \zeta_{rm_{L2}}/\lambda_{L2}\right)\lambda_{\mathrm{WL}} \\ &= \left(\zeta_{rm_{L1}}/\lambda_{L1} - \zeta_{rm_{L1}}/\lambda_{L2} + \zeta_{rm_{L1}}/\lambda_{L2} - \zeta_{rm_{L2}}/\lambda_{L2}\right)\lambda_{\mathrm{WL}} \\ &= \zeta_{rm_{L1}} + \left(\zeta_{rm_{L1}} - \zeta_{rm_{L2}}\right)\frac{f_{L2}}{f_{L1} - f_{L2}} \\ &\approx \zeta_{rm_{L1}} + 3.529 \cdot \left(\zeta_{rm_{L1}} - \zeta_{rm_{L2}}\right)\end{aligned} \tag{6}$$

where $\zeta_{rm_{\mathrm{WL}}}$, $\zeta_{rm_{L1}}$ and $\zeta_{rm_{L2}}$ refer to the IFB rates of the widelane, $L1$ and $L2$ phase observation. c and f_{L1} are the speed of light and the frequency of $L1$ carrier, respectively.

Wanninger (2012) showed that the IFB of the $L1$ band is similar to the $L2$ band, so the value $3.529 \cdot (\zeta_{rm_{L1}} - \zeta_{rm_{L2}})$ will have little impact on the IFB of the widelane observation. We will validate that the IFB of the $L1$ band and $L2$ band only slightly differs, but the value of $3.529 \cdot (\zeta_{rm_{L1}} - \zeta_{rm_{L2}})$ is at the millimeter level or submillimeter level. The difference of the IFB of $L1$ band and widelane observation will not hinder the fixing of GLONASS ambiguity or the new algorithm for GLONASS IFB rate estimation. So, we verified that the IFB of widelane observation is equal to the IFB of $L1$ approximately.

Because the wavelength of widelane observation is four times that of $L1$ observation and the IFB of the widelane is equal to the IFB of $L1$ approximately, the influence of the IFB on the widelane ambiguity fixing is smaller than that on the $L1$ ambiguity fixing. In order to fix the GLONASS widelane ambiguity, the impact of IFB on the widelane DD observation should be within an interval of -0.5 to 0.5 in units of cycle. The GLONASS frequency number ranges between -7 and 7; thus, the difference of two GLONASS satellites frequency numbers is between -14 and 14. If the IFB rate is restricted within -3 to 3 (cm/FN), it would be possible to fix the ambiguity of the widelane observation.

Many parameters, such as ambiguities, IFB rate and coordinates, make it hard to estimate the precise float ambiguities of widelanes. Therefore, a fixed solution of GPS RTK is needed for GLONASS widelane ambiguity fixing and IFB rate estimation. Given the known and precise coordinates computed by a GPS RTK fixed solution, the GLONASS widelane float ambiguity can be calculated as follows:

$$\bar{N}^{ij}_{rm_{\mathrm{WL}}} = (\phi^{ij}_{rm_{WL}} - \rho^{ij}_{rm} - (\lambda^i - \lambda^j)N^j_{rm_{\mathrm{WL}}})/\lambda^i \tag{7}$$

From (7), the main error of the GLONASS widelane float DD ambiguity $\bar{N}^{ij}_{rm_{\mathrm{WL}}}$ is the geometric range error and the IFB.

According to covariance propagation, the influence of geometric range error on float widelane ambiguity is approximately equal to 1.35 times the geometric range error, which can be derived from (7) as follows:

$$\sigma_{\bar{N}_{WL}} = \sqrt{\sigma^2_\rho/\lambda^2_{\mathrm{WL}}} \approx \sqrt{\sigma^2_\rho/(0.86)^2} = 1.35\sigma_\rho \tag{8}$$

where $\sigma_{\bar{N}_{\mathrm{WL}}}$ and σ_ρ refer to the error of widelane float DD ambiguity and DD distance, and λ_{WL} is the wavelength of widelane, which is approximately 86 cm.

Due to the centimeter-level accuracy of the GPS RTK fixed resolution, the effect of the geometric range error on the widelane float ambiguity is less than 0.1 cycles. Thus, the influence of the IFB and geometric range error is less than 0.5 cycles, and the widelane float DD ambiguity $\bar{N}^{ij}_{rm_{\mathrm{WL}}}$ can be fixed to its nearest integer $\breve{N}^{ij}_{rm_{\mathrm{WL}}}$.

Based on GPS and GLONASS widelane integer DD ambiguities and widelane DD phase observations, one can estimate the coordinates and IFB rate. The observation equation can be written as follows:

$$\begin{aligned}\Phi^{ij,\mathrm{GPS}}_{rm_{\mathrm{WL}}} &= \rho^{ij}_{rm} + \lambda\breve{N}^{ij}_{rm_{\mathrm{WL}}} + \varepsilon\left(\Phi^{ij,\mathrm{GPS}}_{rm_{\mathrm{WL}}}\right) \\ \Phi^{ij,\mathrm{GLO}}_{rm_{\mathrm{WL}}} &= \rho^{ij}_{rm} + \lambda^i\breve{N}^{ij}_{rm_{\mathrm{WL}}} + (\lambda^i - \lambda^j)N^j_{rm_{\mathrm{WL}}} + (k^i - k^j)\zeta_{rm_{\mathrm{WL}}} \\ &\quad + \varepsilon\left(\Phi^{ij,GLO}_{rm_{\mathrm{WL}}}\right)\end{aligned} \tag{9}$$

where the IFB of the widelane observation $\zeta_{rm_{\mathrm{WL}}}$ can be estimated accurately, due to the known GPS and GLONASS widelane integer DD ambiguities.

Because the IFB of the widelane observation is approximately equal to that of the $L1$ and $L2$ bands, with the IFB rate estimated by widelane observation $\zeta_{rm_{\mathrm{WL}}}$, the

coordinates and the $L1$ and $L2$ float DD ambiguities of GPS and GLONASS can be estimated by:

$$\begin{aligned}
P_{rm_{L1}}^{ij,\mathrm{GPS}} &= \rho_{rm}^{ij} + \varepsilon\left(P_{rm_{L1}}^{ij,\mathrm{GPS}}\right)\\
P_{rm_{L2}}^{ij,\mathrm{GPS}} &= \rho_{rm}^{ij} + \varepsilon\left(P_{rm_{L2}}^{ij,\mathrm{GPS}}\right)\\
\Phi_{rm_{L1}}^{ij,\mathrm{GPS}} &= \rho_{rm}^{ij} + \lambda_{L1}N_{rm_{L1}}^{ij,\mathrm{GPS}} + \varepsilon\left(\Phi_{rm_{L1}}^{ij,\mathrm{GPS}}\right)\\
\Phi_{rm_{L2}}^{ij,\mathrm{GPS}} &= \rho_{rm}^{ij} + \lambda_{L2}N_{rm_{L2}}^{ij,\mathrm{GPS}} + \varepsilon\left(\Phi_{rm_{L2}}^{ij,\mathrm{GPS}}\right)\\
P_{rm_{L1}}^{ij,\mathrm{GLO}} &= \rho_{rm}^{ij} + \varepsilon\left(P_{rm_{L1}}^{ij,\mathrm{GLO}}\right)\\
P_{rm_{L2}}^{ij,\mathrm{GLO}} &= \rho_{rm}^{ij} + \varepsilon\left(P_{rm_{L2}}^{ij,\mathrm{GLO}}\right)\\
\Phi_{rm_{L1}}^{ij,\mathrm{GLO}} &= \rho_{rm}^{ij} + \lambda_{L1}^{i}N_{rm_{L1}}^{ij,\mathrm{GLO}} + \left(\lambda_{L1}^{i} - \lambda_{L1}^{j}\right)N_{rm_{L1}}^{j,\mathrm{GLO}}\\
&\quad + \left(k^{i} - k^{j}\right)\zeta_{rm_{WL}} + \varepsilon\left(\Phi_{rm_{L1}}^{ij,\mathrm{GLO}}\right)\\
\Phi_{rm_{L2}}^{ij,\mathrm{GLO}} &= \rho_{rm}^{ij} + \lambda_{L2}^{i}N_{rm_{L2}}^{ij,\mathrm{GLO}} + \left(\lambda_{L2}^{i} - \lambda_{L2}^{j}\right)N_{rm_{L2}}^{j,\mathrm{GLO}}\\
&\quad + \left(k^{i} - k^{j}\right)\zeta_{rm_{WL}} + \varepsilon\left(\Phi_{rm_{L2}}^{ij,\mathrm{GLO}}\right)
\end{aligned} \tag{10}$$

Using the observations of (10), the IFB rate estimated by the widelane term $\zeta_{rm_{WL}}$ is used for the GPS + GLONASS $L1 + L2$ DD ambiguity estimation.

Following the process of normal GPS RTK, we use the LAMBDA method to fix the $L1$ and $L2$ float DD ambiguities of GPS and GLONASS (Teunissen 1995). If the fixed ambiguity passes the ratio test (Teunissen 2004), the IFB rate $\zeta_{rm_{L1+L2}}$ and coordinate parameters can be estimated again with the GPS + GLONASS $L1 + L2$ integer DD ambiguity and DD phase observation. The observation equation can be expressed as follows:

$$\begin{aligned}
\Phi_{\mathrm{rm_{L1}}}^{\mathrm{ij,GPS}} &= \rho_{rm}^{ij} + \lambda_{L1}\breve{N}_{rm_{L1}}^{ij,\mathrm{GPS}} + \varepsilon\left(\Phi_{rm_{L1}}^{ij,\mathrm{GPS}}\right)\\
\Phi_{rm_{L2}}^{ij,\mathrm{GPS}} &= \rho_{rm}^{ij} + \lambda_{L2}\breve{N}_{rm_{L2}}^{ij,\mathrm{GPS}} + \varepsilon\left(\Phi_{rm_{L2}}^{ij,\mathrm{GPS}}\right)\\
\Phi_{rm_{L1}}^{ij,\mathrm{GLO}} &= \rho_{rm}^{ij} + \lambda_{L1}^{i}\breve{N}_{rm_{L1}}^{ij,\mathrm{GLO}} + \left(\lambda_{L1}^{i} - \lambda_{L1}^{j}\right)N_{rm_{L1}}^{j,\mathrm{GLO}}\\
&\quad + \left(k^{i} - k^{j}\right)\zeta_{rm_{L1+L2}} + \varepsilon\left(\Phi_{rm_{L1}}^{ij,\mathrm{GLO}}\right)\\
\Phi_{rm_{L2}}^{ij,\mathrm{GLO}} &= \rho_{rm}^{ij} + \lambda_{L2}^{i}\breve{N}_{rm_{L2}}^{ij,\mathrm{GLO}} + \left(\lambda_{L2}^{i} - \lambda_{L2}^{j}\right)N_{rm_{L2}}^{j,\mathrm{GLO}}\\
&\quad + \left(k^{i} - k^{j}\right)\zeta_{rm_{L1+L2}} + \varepsilon\left(\Phi_{rm_{L2}}^{ij,\mathrm{GLO}}\right)
\end{aligned} \tag{11}$$

where the IFB rate parameter of the $L1$ phase observation is the same as for the $L2$ phase observation, which is implied by the symbol $\zeta_{rm_{L1+L2}}$.

Based on different accuracy demands and applications, the IFB rate $\zeta_{rm_{\mathrm{WL}}}$ and $\zeta_{rm_{L1+L2}}$ can be estimated with single-epoch GPS + GLONASS phase observation using least squares adjustment (single-epoch IFB rate estimation) or can be estimated with all epoch data using the Kalman filter (Kalman filter-based IFB rate estimation). For example, RTK positioning needs to estimate the IFB rate in real time. Therefore, single-epoch IFB rate estimation is appropriate for RTK positioning. For millimeter-level accuracy of GLONASS positioning, the estimation accuracy of the IFB rate is crucial, and real-time computation is less important. Therefore, the Kalman filter-based IFB rate estimation would be a reasonable alternative.

A new reference satellite selection method is discussed below, and it is used only when we estimate the approximate IFB rate of the widelane observation.

New reference satellite selection method

There is a problem with the above algorithm when the IFB rate is larger than 3 cm/FN. In this case, the IFB effect on the float widelane ambiguity is more than 0.5 cycles, and the algorithm becomes unusable.

To solve this problem, a new reference satellite selection method is proposed. According to Wanninger (2012), the IFB rate usually is within an interval of [−0.10, 0.10] in units of meters per frequency number (m/FN). To make the IFB error in units of meters less than half the widelane wavelength, the difference in the frequency number between the GLONASS observed satellite and GLONASS reference satellite should be restricted from −4 to 4. Instead of choosing the satellite with the highest elevation angle, we select the reference satellite for each GLONASS satellite based on the principle that the difference in the frequency number between the GLONASS observed satellite and GLONASS reference satellite should be minimized. In general, there are at least four GLONASS satellites tracked for a baseline, and the GLONASS satellite frequency number ranges from −7 to 7. In theory, the minimum difference of the frequency number is maximum when the frequency numbers of four satellites are −7, −2, 2, 7, and the differences of frequency number are 5, 4, 5. Thus, using the new selection method, there is at least one GLONASS DD observation whose difference in the frequency number is less than 5. Using all GPS widelane observations and all GLONASS widelane observation whose difference in the frequency number is < 5, we can estimate the approximate value of the IFB rate $\zeta_{rm_{\mathrm{PRE}}}$ by (9). With that approximate IFB rate $\zeta_{rm_{\mathrm{PRE}}}$, the major effect of the IFB error can be reduced for all GLONASS widelane DD phase observations as follows:

$$\bar{N}_{rm_{\mathrm{WL}}}^{ij} = \left(\phi_{rm_{\mathrm{WL}}}^{ij} - \rho_{rm}^{ij} - (\lambda^{i} - \lambda^{j})N_{rm_{\mathrm{WL}}}^{j} - (k^{i} - k^{j})\zeta_{rm_{\mathrm{PRE}}}\right)/\lambda^{i} \tag{12}$$

Equation (12) shows that the main errors of the GLONASS widelane float DD ambiguity $\bar{N}_{rm_{\mathrm{WL}}}^{ij}$ are geometric range error and residual error of IFB.

Then, the GLONASS widelane DD ambiguity can be fixed well, without the major effect of IFB. Finally, the IFB

rate $\zeta_{rm_{\mathrm{WL}}}$, based on the widelane observation and the IFB rate $\zeta_{rm_{L1+L2}}$ based on $L1 + L2$ observations, can be estimated.

Procedure of the new algorithm

Based on the above definition, the procedures of the single-epoch IFB rate estimation algorithm and the Kalman filter-based IFB rate estimation algorithm can be carried out as follows:

The single-epoch IFB rate estimation algorithm will be discussed first, and the flowchart of this procedure is shown in Fig. 1.

1. The accurate coordinates of the rover receiver should be obtained by the GPS RTK fixed solution. If the GPS ambiguity cannot be fixed in epoch k, repeat this step for epoch $k + 1$ until accurate coordinates can be estimated.
2. Using the new reference satellite selection method, one can choose a reference satellite for each GLONASS satellite tracked. The GLONASS widelane DD ambiguities, which satisfy the condition that the difference of the frequency number should be less than 5, and all GPS widelane DD ambiguities will be fixed to the nearest integer. Using least squares adjustment and (9), the approximate IFB rate $\zeta_{rm_{\mathrm{PRE}}}$ can be estimated with the qualified GLONASS and all GPS integer ambiguities and widelane phase observations.
3. For all GLONASS widelane phase observations, the GLONASS widelane DD ambiguity can be fixed well, without the major effect of the IFB, which can be reduced by using the approximate IFB rate $\zeta_{rm_{\mathrm{PRE}}}$ and (12).
4. Based on GPS and GLONASS widelane integer ambiguities, the widelane phase observations and (9), one can estimate the coordinate parameters and IFB rate $\zeta_{rm_{\mathrm{WL}}}$.
5. With the IFB rate $\zeta_{rm_{\mathrm{WL}}}$ estimated by widelane observation, the coordinates and $L1$ and $L2$ float DD ambiguities of GPS and GLONASS can be estimated by (10).
6. Use LAMBDA to fix the $L1$ and $L2$ float DD ambiguities of GPS and GLONASS. If the fixed ambiguity can pass the ratio test, go to step 7 else repeat steps 1–6 for epoch $k + 1$.
7. Using (11), the IFB rate $\zeta_{rm_{L1+L2}}$ and coordinate parameters can be estimated with the GPS + GLONASS $L1 + L2$ integer ambiguities and phase observations.

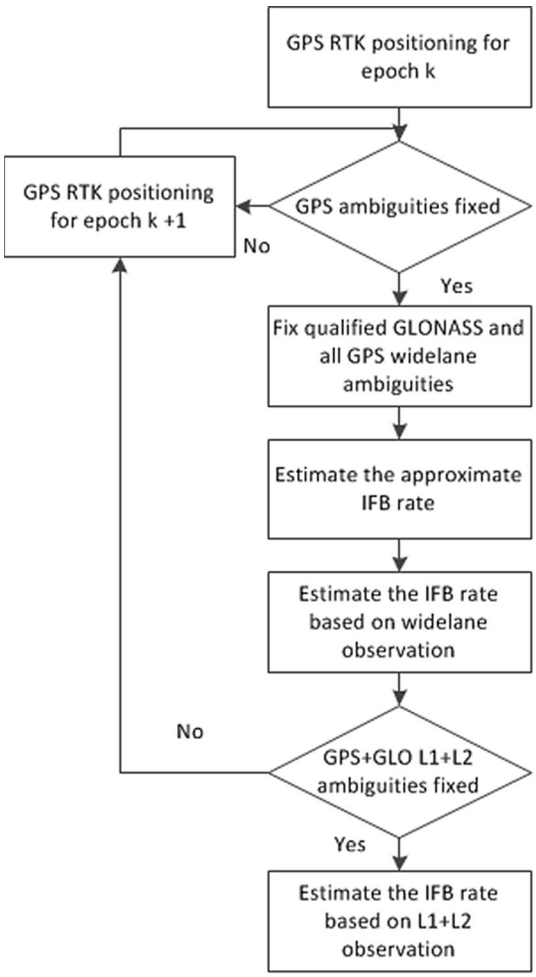

Fig. 1 Flowchart for single-epoch IFB rate estimation algorithm

It should be noted that for typical RTK positioning, we estimate only one IFB rate in the first epoch by the single-epoch IFB rate estimation algorithm. We could then use this IFB rate to eliminate the IFB error in all other epochs. However, in order to assess the performance of single-epoch IFB rate estimation algorithm, we estimate the IFB rate for each epoch data in this study. One should further note that the GPS RTK fixed solution is needed to estimate IFB rate only in the first epoch. With the estimated IFB rate, we could fix the GPS/GLONASS ambiguity in those epochs when GPS ambiguities cannot be fixed.

The Kalman filter-based IFB rate estimation algorithm is presented, and the flowchart of this procedure is shown in Fig. 2.

1. Before estimating the IFB rate, the parameter vectors $\boldsymbol{X_{PRE}}$, $\boldsymbol{X_{WL}}$ and $\boldsymbol{X_{L1+L2}}$ and the variance–covariance matrix of parameters $\boldsymbol{P_{PRE}}$, $\boldsymbol{P_{WL}}$ and $\boldsymbol{P_{L1+L2}}$ for the approximate IFB rate estimation, the IFB rate estimation based on widelane observation and IFB rate estimation based on $L1 + L2$ observation should be initialized.

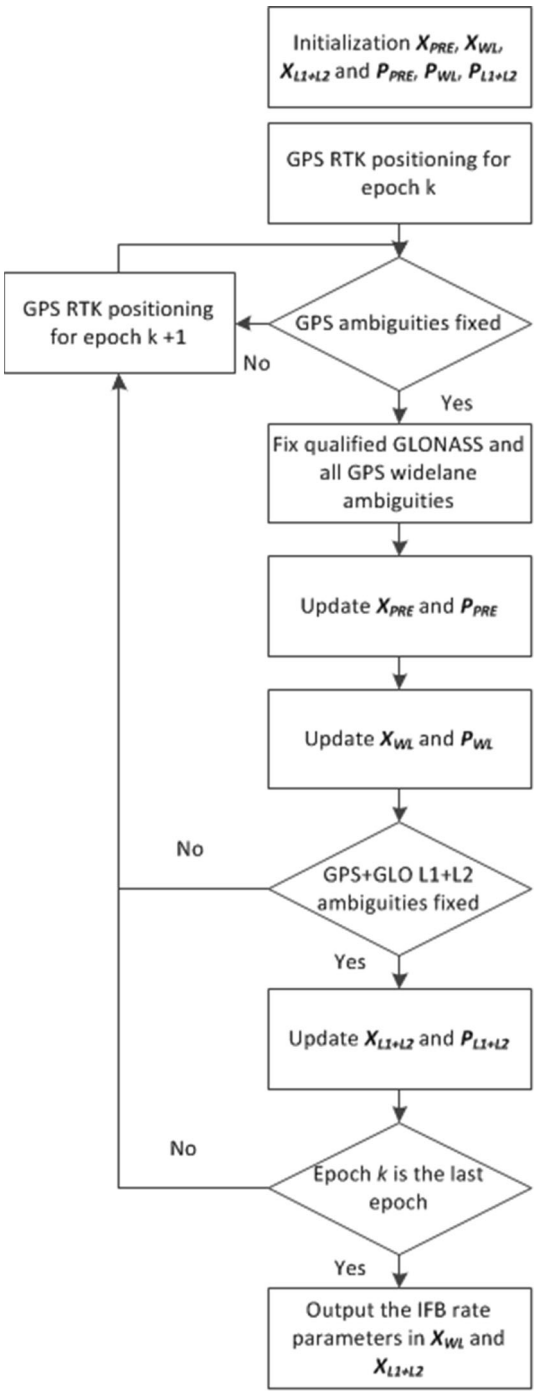

Fig. 2 Flowchart for Kalman filter-based IFB rate estimation algorithm

2. Repeat the first step of the procedure for single-epoch IFB rate estimation algorithm.
3. Using the new reference satellite selection method, the GLONASS widelane DD ambiguities meet the condition that the difference of the frequency number is less than 5, and all GPS widelane DD ambiguities will be fixed to the nearest integer. Using the Kalman filter and (9), $\boldsymbol{X_{PRE}}$ and $\boldsymbol{P_{PRE}}$ can be updated using the qualified GLONASS and all GPS integer widelane ambiguities and widelane phase observation.
4. Using (12) and the approximate IFB rate $\zeta_{rm_{PRE}}$ in $\boldsymbol{X_{PRE}}$, the major effect of the IFB error can be reduced for all GLONASS widelane phase observation. The GLONASS widelane DD ambiguity can be fixed, without the major effect of IFB.
5. Based on GPS and GLONASS widelane integer ambiguities, the widelane phase observations and (9), one can update $\boldsymbol{X_{WL}}$ and $\boldsymbol{P_{WL}}$ by the Kalman filter.
6. Using the IFB rate $\zeta_{rm_{WL}}$ estimated by widelane observation in $\boldsymbol{X_{WL}}$, the coordinates and the $L1$ and $L2$ float DD ambiguities of GPS and GLONASS can be estimated by (10).
7. Use the LAMBDA method to fix the $L1$ and $L2$ float DD ambiguities of GPS and GLONASS. If the fixed ambiguity can pass the ratio test, go to step 8 else repeat steps 1–6 for epoch $k + 1$.
8. Using (11), $\boldsymbol{X_{L1+L2}}$ and $\boldsymbol{P_{L1+L2}}$ can be updated with the GPS + GLONASS $L1 + L2$ integer ambiguities and phase observations.
9. If epoch k is the last epoch, the IFB rate parameters in $\boldsymbol{X_{WL}}$ and $\boldsymbol{X_{L1+L2}}$ are the IFB rate estimated with widelane observation $\zeta_{rm_{WL}}$ and the IFB rate estimated with $L1 + L2$ observation $\zeta_{rm_{L1+L2}}$; else repeat steps 1–8 for epoch $k + 1$.

Experimental validation

To validate the new algorithm, the GNSS baseline observations used in this study are obtained from two receivers designed by different manufacturers. Details are given in Table 1.

For the sake of convenience, we abbreviate the terms single-epoch IFB rate estimation and the Kalman filter-based IFB rate estimation by method 1 and method 2, respectively. IFB rates estimated with widelane observation, $L1$ and $L2$ observation together, $L1$ observation and $L2$ observation are abbreviated as $\zeta_{rm_{\mathrm{WL}}}$, $\zeta_{rm_{L1+L2}}$, $\zeta_{rm_{L1}}$ and $\zeta_{rm_{L2}}$.

Analyzing results of the new algorithm

A phenomenon is observed when all baseline data are processed by the new algorithm, especially for the Kalman filter-based IFB rate estimation. To demonstrate this, baseline observation of STR1–STR2a in DoY 255, 2016 is taken as an example. The IFB rates $\zeta_{rm_{\mathrm{WL}}}$, $\zeta_{rm_{L1+L2}}$, $\zeta_{rm_{L1}}$ and $\zeta_{rm_{L2}}$ are presented in Fig. 3. Wanninger (2012) proved that the IFB rates of $L1$ and $L2$ are equal, so the value of $3.529 \cdot$

Table 1 Details of the test data

	Base			Rover			Sampling interval (s)	Baseline length (km)	Date
	Name	Receiver type	Antenna type	Name	Receiver type	Antenna type			
STR1–STR2a	STR1	SEPT POLARX5	ASH701945C_M	STR2	TRIMBLE NETR9	TRM59800.00	30	0.1	2016 Doy 255
CUT0–CUT1	CUT0	TRIMBLE NETR9	TRM59800.00	CUT1	SEPT POLARX4	TRM59800.00	30	0.0	2015 Doy 337
SMNE–MLVL	SMNE	TRIMBLE NETR9	TRM55971.00	MLVL	LEICA GR25	TRM57971.00	30	11.9	2015 Doy 338
WUHN–ROER	WHUN	TRIMBLE NETR9	TRM59900.00	WHUR	PANDA M1	STNS10	1	<2.0	2016 Doy 356
STR1–STR2b	STR1	SEPT POLARX5	ASH701945C_M	STR2	TRIMBLE NETR9	TRM59800.00	30	0.1	2016 Doy 256
KIRU–KIR8	KIRU	SEPT POLARX4	SEPCHOKE_MC	KIR8	TRIMBLE NETR9	LEIAR25.R3	30	4.5	2016 Doy 209

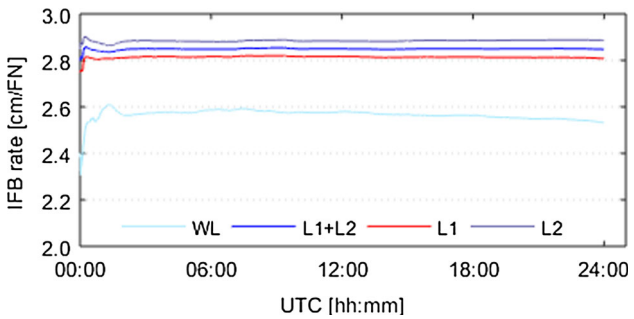

Fig. 3 IFB rates estimated by method 2 with widelane, $L1 + L2$, $L1$ and $L2$ observations for baseline STR1–STR2a

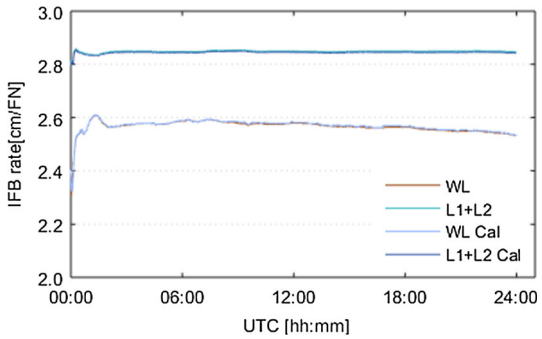

Fig. 4 IFB rate estimated with widelane $L1 + L2$ observation and the IFB rate calculated by IFB rate of $L1$ and IFB rate of $L2$ for baseline STR1–STR2a

$(\zeta_{rm_{L1}} - \zeta_{rm_{L2}})$ should be zero and the IFB rates of the widelane observation and $L1$ observation should be equal as derived from formula (6). In the figure, the IFB rates are not equal, especially the IFB rates $\zeta_{rm_{L1+L2}}$ and $\zeta_{rm_{\mathrm{WL}}}$. It means the value of $3.529 \cdot (\zeta_{rm_{L1}} - \zeta_{rm_{L2}})$ is not equal to zero, and the IFB rates of $L1$ and $L2$ differ. To validate our hypothesis that the IFB rates of $L1$ and $L2$ are different, we used the estimated IFB rates $\zeta_{rm_{L1}}$ and $\zeta_{rm_{L2}}$ to calculate the IFB rate of widelane observation (WL Cal) and the IFB rate estimated with $L1 + L2$ observation ($L1 + L2$ Cal), as follows:

$$\begin{aligned} \zeta_{rm_{\mathrm{WLCal}}} &= (\zeta_{rm_{L1}}/\lambda_{L1} - \zeta_{rm_{L2}}/\lambda_{L2})\lambda_{\mathrm{WL}} \\ \zeta^{\mathrm{Cal}}_{rm_{L1+L2\mathrm{Cal}}} &= (\zeta_{rm_{L1}} + \zeta_{rm_{L2}})/2 \end{aligned} \tag{13}$$

The calculated IFB rates of the widelane observation and $L1 + L2$ observation are present in Fig. 4.

Figure 4 shows that the lines WL and WL Cal, which are calculated by the IFB rates $\zeta_{rm_{L1}}$ and $\zeta_{rm_{L2}}$, are coincident, and that the lines $L1 + L2$ and $L1 + L2$ Cal are also coincident. Therefore, the IFB rate for the $L1$ observation and $L2$ observation is not the same; this inequality is the reason that the IFB rate of widelane observation is different from the IFB rate of $L1 + L2$ observation.

From Fig. 3 and Table 2, the difference between IFB rates $\zeta_{rm_{L1+L2}}$ and those of $\zeta_{rm_{L1}}$, $\zeta_{rm_{L2}}$ is at submillimeter level, and the difference between IFB rates $\zeta_{rm_{WL}}$ and $\zeta_{rm_{L1+L2}}$ is at millimeter level. Because these differences are small, we could use the IFB rates $\zeta_{rm_{\mathrm{WL}}}$ as the a priori value of $\zeta_{rm_{L1+L2}}$ and estimate $\zeta_{rm_{L1+L2}}$ instead of $\zeta_{rm_{L1}}$ and $\zeta_{rm_{L2}}$.

Another analysis is the ambiguity resolution and positioning performance of IFB rates $\zeta_{rm_{\mathrm{WL}}}$, $\zeta_{rm_{L1+L2}}$, $\zeta_{rm_{L1}}$ and $\zeta_{rm_{L2}}$. Table 2 shows the IFB rate estimated by method 2 with widelane, $L1 + L2$, $L1$ and $L2$ observations and its application performance in terms of ambiguity resolution and positioning. It is clear that the performance of the IFB rate estimated with the widelane is weaker than that with $L1$, $L2$ or $L1 + L2$. Although there is a slight difference between the IFB rate of $L1$ and $L2$, one can use the IFB rate $\zeta_{rm_{L1+L2}}$ to obtain the same positioning performance when using the IFB rates $\zeta_{rm_{L1}}$ and $\zeta_{rm_{L2}}$. Therefore, we can

Table 2 Ambiguity resolution and positioning performance with IFB rates estimated with widelane, $L1 + L2$, $L1$ and $L2$ observations by the Kalman filter for baseline STR1–STR2a

IFB rate estimated method	WL	$L1 + L2$	$L1$	$L2$
IFB rate [cm/FN]	2.531	2.847	2.808	2.887
Fixed rate [%]	98.02	98.99	98.99	
Failure rate [%]	0.00	0.00	0.00	
Mean values [cm]				
N	0.30	0.32	0.32	
E	0.60	0.59	0.59	
U	0.47	0.48	0.48	
RMS [cm]				
N	0.73	0.35	0.35	
E	0.66	0.60	0.60	
U	1.02	0.62	0.62	

replace the IFB rates $\zeta_{rm_{L1}}$ and $\zeta_{rm_{L2}}$ with the IFB rate $\zeta_{rm_{L1+L2}}$. Considering the weak positioning performance of the IFB rate $\zeta_{rm_{\mathrm{WL}}}$, it is necessary to estimate the IFB rate using $L1$ and $L2$ observations after $\zeta_{rm_{\mathrm{WL}}}$ has been estimated, and use $\zeta_{rm_{L1+L2}}$ to remove the IFB error in GLONASS ambiguity resolution and positioning. The fixed and failure rates in Table 2 are presented in Teunissen (2005) and Li et al. (2013).

The last analysis focuses on the difference between method 1 and method 2. Evidently, the precision of the IFB rate estimated by method 2, which uses all epoch data, is better than the IFB rate estimated with data from a single epoch, as shown in Fig. 5. The ambiguity resolution and positioning performance of these two methods are discussed based on the RTK positioning of baseline STR1–STR2a. For method 1, the IFB error in each epoch is adjusted by the IFB rates estimated in the corresponding epoch by the single-epoch IFB rate estimation. For method 2, the IFB error in each epoch is adjusted by the IFB rate estimated by the Kalman filter using all epoch data. The statistics are presented in Table 3. The performance of

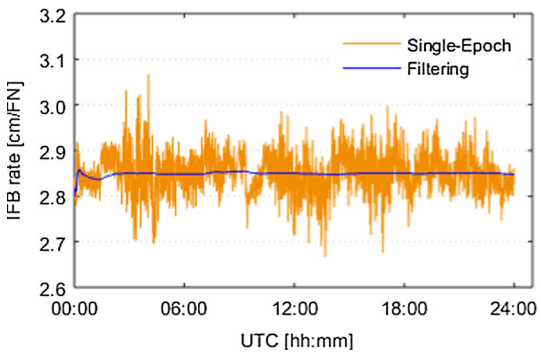

Fig. 5 IFB rates estimated by method 1 and method 2 with the $L1 + L2$ observation for baseline STR1–STR2a

Table 3 Ambiguity resolution and positioning performance of method 1 and method 2 with the $L1 + L2$ observation for baseline STR1–STR2a

IFB rate estimated method	Single epoch	Filtering
Fixed rate [%]	90.00	98.99
Failure rate [%]	0.00	0.00
Mean values [cm]		
N	0.34	0.32
E	0.61	0.59
U	0.47	0.48
RMS [cm]		
N	0.40	0.35
E	0.64	0.60
U	0.66	0.62

method 2 is better than that of method 1, which proves that a more accurate IFB rate can be obtained by method 2. However, the difference in positioning accuracy between these two methods is at submillimeter level in terms of the root-mean-square (RMS), which means that method 1 can meet the precision requirements of RTK positioning. Therefore, in RTK positioning, we can use method 1 to estimate the IFB rate in real time without decreasing the positioning accuracy.

Real-time application of single-epoch IFB rate estimation on RTK positioning

Although method 1 can provide the IFB rate in real time with high accuracy, this method still needs to be validated for different situations. Three baselines, CUT0–CUT1, SMNE–MLVL and WUHN–ROER, which are a zero baseline, a 12-km baseline and a kinematic baseline, respectively, are processed by method 1. Table 4 and Figs. 6, 7 and 8 present the performance of the estimated IFB rate for these baselines. The mean values of the IFB rate show that the IFB rate estimated with widelane observation is not equal to the IFB rate of $L1 + L2$, which proves again that there is a difference among the IFB rate of $L1$ and the IFB rate of $L2$. The IFB rate estimated by method 1 is stable and reliably demonstrated by the IFB rate standard deviation (STD) shown in Table 4 and the IFB rate time series shown in Figs. 6, 7 and 8.

From Figs. 6, 7 and 8, the single-epoch IFB rate is successfully estimated at most epochs by the new algorithm. Using the first single-epoch IFB rate (-0.395, -2.986 cm/FN), the GPS/GLONASS RTK fixed positions for the two static baselines CUT0–CUT1 and SMNE–MLVL are shown in Fig. 9 and Table 5. The GPS/GLONASS RTK fixed positioning results are accurate and reliable for baselines CUT0–CUT1 and SMNE–MLVL.

Table 4 Performance of the IFB rate estimated by the single epoch for baselines CUT0–CUT1, SMNE–MLVL and WUHN–ROER

Data	CUT0–CUT1		SMNE–MLVL		WUHN–ROER	
IFB rate estimated method	WL	$L1 + L2$	WL	$L1 + L2$	WL	$L1 + L2$
Mean values [cm/FN]	−0.361	−0.378	−2.684	2.999	−3.116	−3.084
STD [cm/FN]	0.169	0.032	0.293	0.121	0.344	0.112

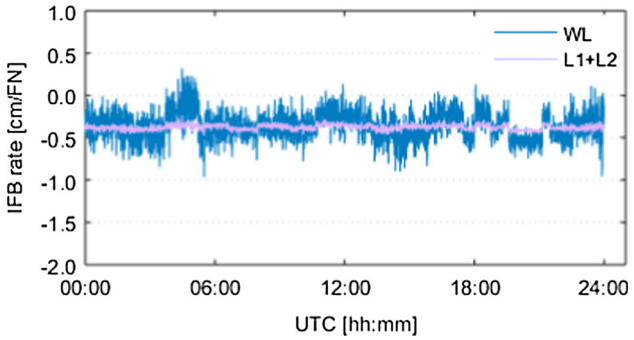

Fig. 6 Time series of the IFB rate estimated with widelane and $L1 + L2$ observation using method 1 for baseline CUT0–CUT1

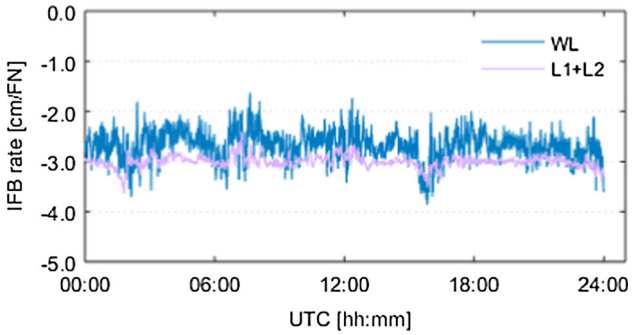

Fig. 7 Time series of the IFB rate estimated with widelane and $L1 + L2$ observation using method 1 for baseline SMNE–MLVL

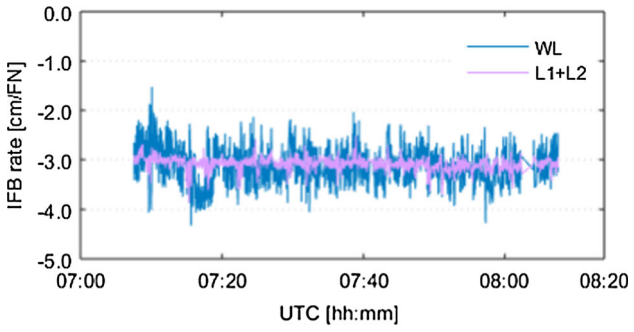

Fig. 8 Time series of the IFB rate estimated with widelane and $L1 + L2$ observation using method 1 for baseline WUHN–ROER

This shows that the IFB rate estimated by the new algorithm is reliable and accurate, even for the baseline with a length of 12 km.

The kinematic baseline WUHN–ROER has been processed as well. Figure 10 shows the project area; the outer edge of the runway is obscured seriously. There are many

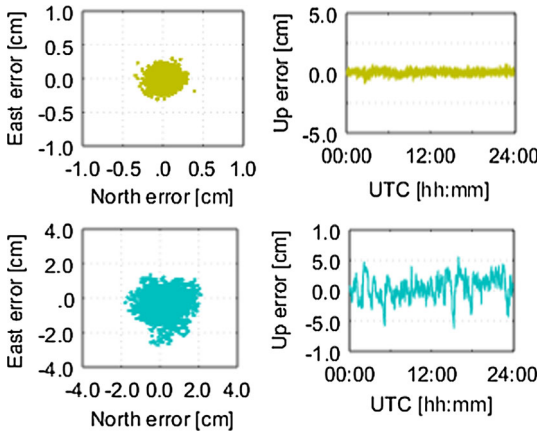

Fig. 9 GPS/GLONASS RTK fixed positioning for the baselines CUT0–CUT1 (*top left* horizontal (N, E) scatterplots, *top right* vertical (U) time series) and SMNE–MLVL (*bottom left* horizontal (N, E) scatterplots, *bottom right* vertical (U) time series)

Table 5 Accuracy statistics of GPS/GLONASS RTK fixed positioning for the baselines CUT0–CUT1 and SMNE–MLVL

Data	CUT0–CUT1			SMNE–MLVL		
	E	N	U	E	N	U
Mean values	0.0	0.0	0.0	−0.3	0.2	0.4
RMS	0.1	0.1	0.2	0.7	0.7	1.9

Units are centimeter

Fig. 10 Environment for the kinematic baseline WUHN–ROER

float solutions for GPS RTK at the outer edge in Fig. 11. The percentage of fixed solution epochs is only 81%. However, using the first single-epoch IFB rate (−3.012 cm/FN) in Fig. 8, the GLONASS DD ambiguity

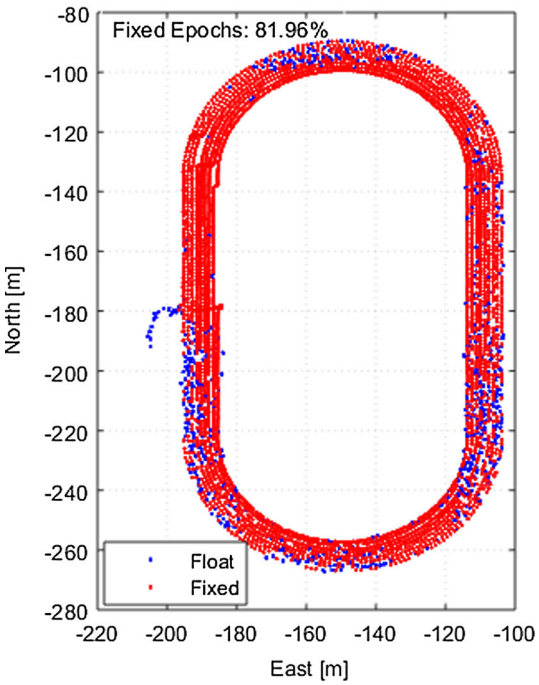

Fig. 11 Fixed and float solutions of GPS RTK positioning for the kinematic baseline WUHN–ROER

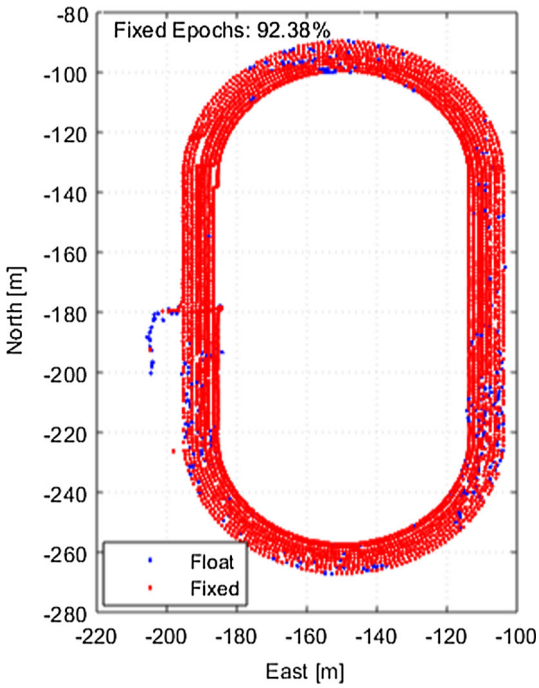

Fig. 12 Fixed and float solutions of GPS/GLONASS RTK positioning using the first single-epoch IFB rate for the kinematic baseline WUHN–ROER

can be fixed, and for the GPS/GLONASS RTK, the percentage of fixed solutions increases distinctly. In Fig. 12, for GPS/GLONASS RTK using the IFB rate, approximately 10% of points of the GPS RTK float solutions at the outer edge of the runway are fixed. Therefore, even if we have GPS RTK, it is necessary to use the GPS RTK fixed solution to estimate the IFB rate, which will help us to obtain more fixed solutions at places with serious occlusion.

IFB rate is larger than 3 cm/FN

According to Wanninger (2012), the differences among manufacturers can reach up to 10 cm for adjacent frequencies. Therefore, we can analyze the performance of the new algorithm in estimating the IFB rate when it is 10 cm/FN. Because baseline data with an IFB rate of 10 cm/FN are rare, we change the IFB rate of the baseline STR1–STR2b from 2.82 to 10.00 cm/FN in the original GNSS observation before estimating the IFB rate. In Fig. 13, the three lines for the single-epoch approximate IFB rate (WL-Pre), single-epoch IFB rate of WL and $L1 + L2$ fluctuate at approximately 10 cm/FN, which means the IFB rate single-epoch estimation is able to estimate an IFB rate of 10 cm/FN. Because the number of qualified GLONASS DD observations is small, the fluctuation range and the RMS of WL-Pre are larger than those of the WL and $L1 + L2$, as shown in the figure and Table 6.

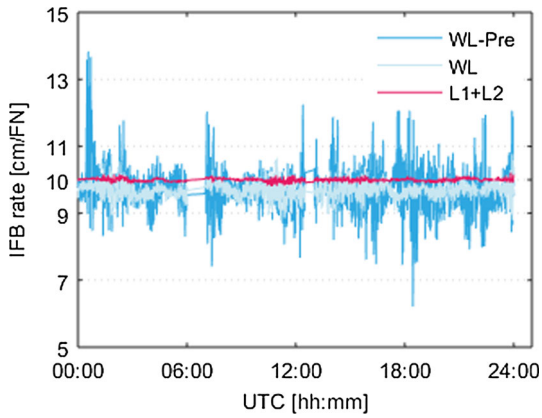

Fig. 13 Single-epoch approximate IFB rate (WL-Pre), single-epoch IFB rate estimated with widelane observation and $L1 + L2$ observations for the baseline STR1–STR2b

Table 6 Statistics of the IFB rate using the IFB rate single-epoch estimation for the baseline STR1–STR2b

IFB rate estimated method	WL-Pre	WL	$L1 + L2$
Mean values [cm/FN]	9.698	9.634	9.999
RMS [cm/FN]	0.618	0.220	0.048

Figure 14 and Table 7 shows that method 2 can exactly estimate the IFB rate, which is 10 cm/FN. Due to the inequality between the IFB rates of $L1$ and $L2$, there is a

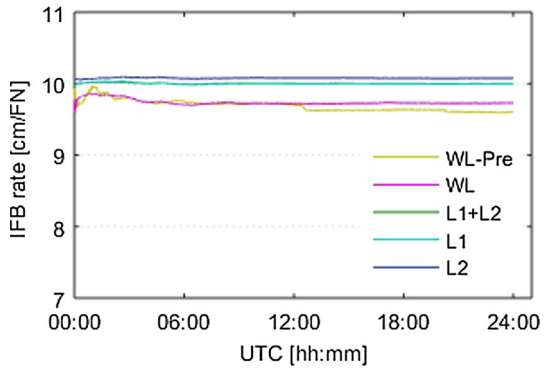

Fig. 14 Approximate IFB rate (WL-Pre) and IFB rates estimated with widelane observation (WL) and $L1 + L2$ observation ($L1 + L2$) by method 2 for the baseline STR1–STR2b

Table 7 Results of method 2 for the baseline STR1–STR2b

IFB rate estimated method	IFB rate [cm/FN]
WL-Pre	9.01
WL	9.73
$L1 + L2$	10.00
$L1$	10.00
$L2$	10.08

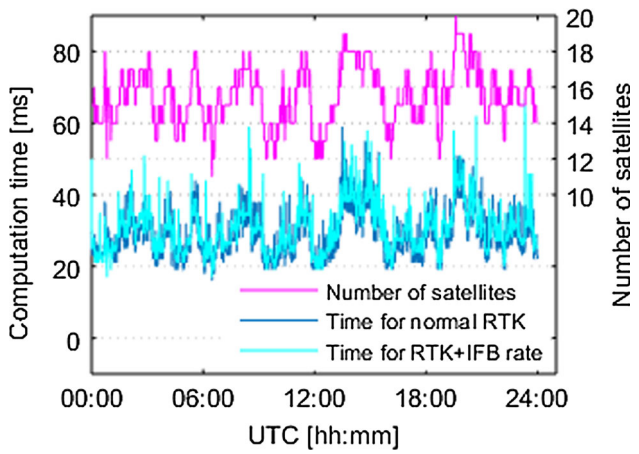

Fig. 15 Relationship between the number of satellites, the time for normal GPS/GLONASS RTK and time for GPS/GLONASS RTK with single-epoch IFB rate estimation

difference between the IFB rate estimated with widelane observation (lines WL and WL-Pre) and the IFB rate estimated with $L1$ and $L2$ (lines $L1$, $L2$ and $L1 + L2$), as shown in the figure and table.

Computational efficiency

Since the data processing capability of the GNSS receiver cannot reach that of a personal computer, the computational time of the new algorithm is crucial for its application in actual RTK positioning. Thus, the baseline data KIRU–KIR8 are processed to obtain the computational time of the new algorithm (single-epoch IFB rate estimation case). Figure 15 shows the relationship between the number of satellites, the time for normal GPS/GLONASS RTK, and the time for GPS/GLONASS RTK with single-epoch IFB rate estimation at each epoch. The time for GPS/GLONASS RTK with single-epoch IFB rate estimation is slightly larger than the time for normal GPS/GLONASS RTK. The total computational time for normal GPS/GLONASS RTK is 79158 s, and the GPS/GLONASS RTK with single-epoch IFB rate estimation is 85501 s. Therefore, we can obtain the GPS/GLONASS RTK fixed solution, which is more accurate, with only 8% extra computational time.

Conclusions

Because GLONASS DD ambiguity resolution is adversely impacted by the IFB, removing or eliminating the impact of the IFB error is important for accurate positioning with GLONASS. In this study, a new algorithm for IFB rate estimation is proposed. The widelane wavelength is several times that of the $L1$ observation, but both have similar IFB errors in units of meters. Thus, the IFB effect on widelane observation can be restricted within 0.5 cycles with the new algorithm. The widelane DD ambiguity can be fixed, and the IFB rate can be estimated with the widelane fixed ambiguity and phase observation. Due to the low accuracy of the IFB rate estimated with widelane observations, the new algorithm needs to refine the estimate of the IFB rate with widelane and $L1 + L2$ observation. Two IFB rate estimation methods are presented. For real-time applications, the single-epoch IFB rate estimation can provide the real-time IFB rate with sufficient accuracy in most epochs. For high-accuracy applications, the Kalman filter-based IFB rate estimation will meet the requirements.

The new algorithm is validated by several experiments. In the first one, the result shows that the IFB rates on $L1$ and $L2$ bands are different, which leads to the difference in the IFB rate estimated by widelane observation and the IFB rate estimated by $L1 + L2$ observation. Another conclusion is that we have to estimate the IFB rate with $L1 + L2$ observation, because of the low accuracy for the IFB rate estimated from widelane observation. The last conclusion from our first experiment is that the positioning accuracy using the single-epoch estimated IFB rate is lower than the Kalman filter-based IFB rate estimation, but it is enough for RTK positioning. The other experiment used three baselines, a zero baseline, a 12-km baseline and a kinematic baseline to validate the performance of the single-

epoch IFB rate estimation. The result shows that the single-epoch IFB rate estimation is available for different situations. The third and fourth experiments prove that the new algorithm is available even if the IFB rate is 10 cm/FN, and that the computational efficiency of the new algorithm is acceptable.

Acknowledgements This work is supported by the National Key Research and Development Program of China (No. 2016YFB0501803). The GNSS datasets were collected from the EUREF Permanent Network and MGEX in this study: The support from these organizations is acknowledged.

References

Al-Shaery A, Zhang S, Rizos C (2013) An enhanced calibration method of GLONASS inter-channel bias for GNSS RTK. GPS Solut 17(2):165–173

Li B, Shen Y, Feng Y, Gao W, Yang L (2013) GNSS ambiguity resolution with controllable failure rate for long baseline network RTK. J Geod 88(2):99–112

Pratt M, Burke B, Misra P (1998) Single-epoch integer ambiguity resolution with GPS–GLONASS *L*1–*L*2 Data. Approach Control 1999:691–699

Takasu T, Yasuda A (2009) Development of the low-cost RTK-GPS receiver with an open source program package RTKLIB. In: International symposium on GPS/GNSS. Seogwipo-si Jung-mun-dong, Korea, 4–6 Nov

Teunissen PJG (1995) The least squares ambiguity decorrelation adjustment: a method for fast GPS integer estimation. J Geod 70(1):65–82

Teunissen PJG (2004) Penalized GNSS ambiguity resolution. J Geod 78(4–5):235–244

Teunissen PJG (2005) Integer aperture bootstrapping: a new GNSS ambiguity estimator with controllable fail-rate. J Geod 79(6):389–397

Tian Y, Ge M, Neitzel F (2015) Particle filter-based estimation of inter-frequency phase bias for real-time GLONASS integer ambiguity resolution. J Geod 89(11):1145–1158

Wang J (2000) An approach to GLONASS ambiguity resolution. J Geod 74(5):421–430

Wanninger L (2012) Carrier-phase inter-frequency bias of GLONASS receivers. J Geod 86(2):139–148

Wanninger L, Wallstab-Freitag S (2007) Combined processing of GPS, GLONASS, and SBAS code phase and carrier phase measurements. J Geod 86(2):139–148

Yibin Yao is currently a Professor at School of Geodesy and Geomatics, Wuhan University. He obtained his Ph.D. in Geodesy and Surveying Engineering from the Wuhan University in 2004. His current research interest is in the GNSS ionospheric/atmospheric/meteorological studies and high-precision GNSS data processing.

Mingxian Hu is a Master Student at School of Geodesy and Geomatics, Wuhan University, China. He obtained his B.Sc. degree in 2014. His current researches are focused on the algorithm research on real-time GNSS precise positioning technology.

Xiayan Xu is a postgraduate student of GNSS Research Center at Wuhan University, who is the candidate of the national foundation named the new method of GEO/IGSO/MEO orbit and clock combination. Her current research interests include GNSS data processing and the orbit and clock combination.

Yadong He is a Master Student at the Wuhan University. He obtained his B.Sc. degree in 2014. His current research focuses mainly involve real-time GNSS precise positioning technology.